Optics Letters

Deterministic aperiodic photonic crystal nanobeam supporting adjustable multiple mode-matched resonances

Jingxuan Wei,[1,2,3] Fujun Sun,[1,2,4] Bowei Dong,[1,2,3] Yiming Ma,[1,2,3] Yuhua Chang,[1,2,3] Huiping Tian,[4] and Chengkuo Lee[1,2,3,*]

[1]Department of Electrical and Computer Engineering, National University of Singapore, Singapore 117583, Singapore
[2]Center for Intelligent Sensors and MEMS, National University of Singapore, 5 Engineering Drive 1, Singapore 117608, Singapore
[3]NUS Suzhou Research Institute (NUSRI), Suzhou Industrial Park, Suzhou 215123, China
[4]State Key Laboratory of Information Photonics and Optical Communications, School of Information and Communication Engineering, Beijing University of Posts and Telecommunications, Beijing 100876, China
*Corresponding author: elelc@nus.edu.sg

Received 10 September 2018; revised 3 October 2018; accepted 4 October 2018; posted 5 October 2018 (Doc. ID 345484); published 29 October 2018

We investigate nanocavities in deterministic aperiodic photonic crystal (PhC) nanobeams. We reveal that even a single nanocavity can support multiple mode-matched resonances, which show an almost perfect field overlap in the cavity region. The unique property is enabled by the existence of adjustable multiple bandgaps in deterministic aperiodic PhC nanobeams. Our investigation may inspire related studies on low threshold lasers, integrated nonlinear devices, optical filters, and on-chip sensors.

https://doi.org/10.1364/OL.43.005407

Photonic crystal (PhC) nanobeams are compact on-chip one-dimensional dielectric waveguides that confine light in the transverse directions and have photonic bandgaps along their propagation direction [1,2]. Conceptually similar to a Fabry–Pérot cavity consisting of an optical cavity surrounded by two Bragg mirrors, nanocavities in nanobeams can also be designed deterministically and achieve high quality (Q) factors and small mode volumes [3]. By merit of their unique properties, nanocavities have been widely used in various areas such as integrated nanoscale emitters [4,5], cavity optomechanics [6], on-chip single particle sensing [7], and interconnects applications [8]. Besides, it has long been desired to achieve multiple field-matched resonances in a single nanocavity for applications such as multiple narrowband light sources and integrated nonlinear devices [4,9]. Traditionally, multimode nanocavities are obtained by increasing the cavity length [10]. While the fundamental mode is confined at the center, field distribution of the higher-order mode shifts away, making the overall field overlap between different modes negligible. Another potential alternative is to use both dielectric and air modes in a tapered nanocavity; however, since dielectric and air modes are mainly focused in the dielectric and air regions, respectively, the overlap between the two types of modes is also limited [7,11]. Modes with different orthogonal polarizations can be supported in a single nanocavity, but the different polarizations also limit the field overlap [12]. Besides, coupled PhC nanocavities show two energy-split modes, which also possess opposite symmetry [13]. Therefore, it still remains challenging to design a nanocavity that can support multiple resonances with a significant field overlap.

On the other hand, since the surprising discovery of quasicrystal by Shechtman in 1984, researchers have revealed that nonperiodic structures own unique properties that may not be possessed by periodic structures [14]. Although nonperiodic structures, in general, lack translational symmetry, they can possess a long-range order [15]. The uniqueness of the nonperiodic structure is revealed in a clearer way when we look at the Fourier transform of the geometrical structures. In contrast to periodic structures that show only one dominant Fourier component, rich Fourier spectra have been found in nonperiodic structures such as Fibonacci, Tue–Morse, Rudin–Shapiro, and period-doubling sequences[14]. Another research direction in nonperiodic PhC is deterministic design by simply summing multiple periodic structures logically [16,17]. Although parasitic bandgaps are usually expected, this method provides an intuitive way to design the structure in Fourier space. Since the discrete components contribute to the formation of bandgaps, which further have an impact on resonances in a nanocavity, we anticipate that the problem of multiple mode-matched resonances in a single nanocavity could be solved using nonperiodic PhC nanobeams [14,18].

In this Letter, we report on the design of deterministic aperiodic PhC nanobeam structures which possess two discrete adjustable components in Fourier space. Both simulation and experimental results confirm the existence of two distinct bandgaps in the nanobeams. This Letter suggests that there is

no interference between the reflection phase responses from the two bandgaps. Within each bandgap, the reflection phase response changes almost linearly from π to 0 when the wavelength sweeps from the shorter wavelength edge to the longer wavelength edge, which agrees with the previous studies [18]. One resonance exists in each bandgap, the mode orders of which are confirmed to be the same by (FDTD) simulation and experimental results. The calculated field overlap efficiency of the two resonances in the gap region is nearly perfect. We envision that this Letter offers opportunities for integrated nonlinear optics, filters, multiple wavelength light sources, slow light engineering, and on-chip sensing.

Figure 1 shows a schematic illustration of our design concept. We first start from a single periodic structure, as shown in Fig. 1(a). A nanobeam is plotted in gray with white rectangles as etched holes with a period of P. Figures 1(b) and 1(c) show the typical effective refractive index (n_{eff}) profile and Fourier components of a conventional periodic nanobeam, respectively. Here we have assumed that holes can be regarded as perturbation. Then the process of Fourier transform can be expressed by

$$\mathrm{FT}\left\{\mathrm{III}_P(x) * \mathrm{rect}\left(\frac{x}{a}\right)\right\} = \frac{a}{P}\mathrm{III}_{\frac{1}{P}}(f)\cdot\mathrm{sinc}(af), \quad \textbf{(1)}$$

where $\mathrm{III}_p(x)$, $\mathrm{rect}(x)$, and $\mathrm{sinc}(x)$ denote the comb function with a period of P, rectangle function, and sinc function, respectively. a is the width of the rectangle function. FT represents the Fourier transform operator. $*$ denotes the operation of convolution. Due to the existence of distinct Fourier components in Fig. 1(c), a bandgap will appear at the edge of the Brillouin zone in the dispersion, as shown in Fig. 1(d). The width of the bandgap in Fig. 1(d) is proportional to the intensity of the Fourier component in Fig. 1(c) [2]. After we have been familiar with the case of a periodic PhC nanobeam, we move to deterministic aperiodic PhC structure, as shown in Fig. 1(e). Figures 1(f) and 1(g) show the effective index profile and calculated Fourier components, respectively. From Fig. 1(g), we can obviously see two strong Fourier components, which are related to the formation of two bandgaps, as illustrated in Fig. 1(h). The Fourier transform of the index profile of an aperiodic PhC nanobeam is given by

$$\mathrm{FT}\left\{\mathrm{III}_{P_1}(x) * \mathrm{rect}\left(\frac{x}{a_1}\right) + \mathrm{III}_{P_2}(x) * \mathrm{rect}\left(\frac{x}{a_2}\right)\right\} = \frac{a_1}{P_1}\mathrm{III}_{\frac{1}{P_1}}(f)\cdot\mathrm{sinc}(a_1 f) + \frac{a_2}{P_1}\mathrm{III}_{\frac{1}{P_1}}(f)\cdot\mathrm{sinc}(a_2 f). \quad \textbf{(2)}$$

From both Fig. 1(g) and Eq. (2), we confirm that there are no parasitic Fourier components, and the Fourier components are just a simple summation of the two periodic structures.

As the first step, we design aperiodic nanobeams with multiple adjustable bandgaps using commercially available FDTD software (Lumerical). The width of the silicon nanobeam is set to be 1.2 μm, and the thickness of the device layer is 500 nm. The holes are rectangles with a lateral length of 250 nm. Since the range of our laser source is limited, we have intentionally designed narrow photonic bandgaps by shifting holes away from the center of a nanobeam. The distance between the center line of the nanobeam and the center of the hole is 0.6 μm. The designed devices are then fabricated on a commercial silicon-on-insulator wafer using standard electron beam lithography followed by reactive ion plasma etching. Grating couplers are designed to couple light in and out of the nanobeam, which has been reported in our previous work [19]. Figure 2(a) shows the numerical and experimental results for aperiodic structures with two periods of 0.96 and 1 μm. In the figure, we can see that there are two distinct bandgaps covering from 3.79 to 3.82 μm and from 3.86 to 3.89 μm, and simulated results match well with measured data. The bandwidths of the two photonic bandgaps are almost the same, since the two arrays of holes are designed to possess the same size. In Fig. 2(b), we experimentally demonstrate that the two

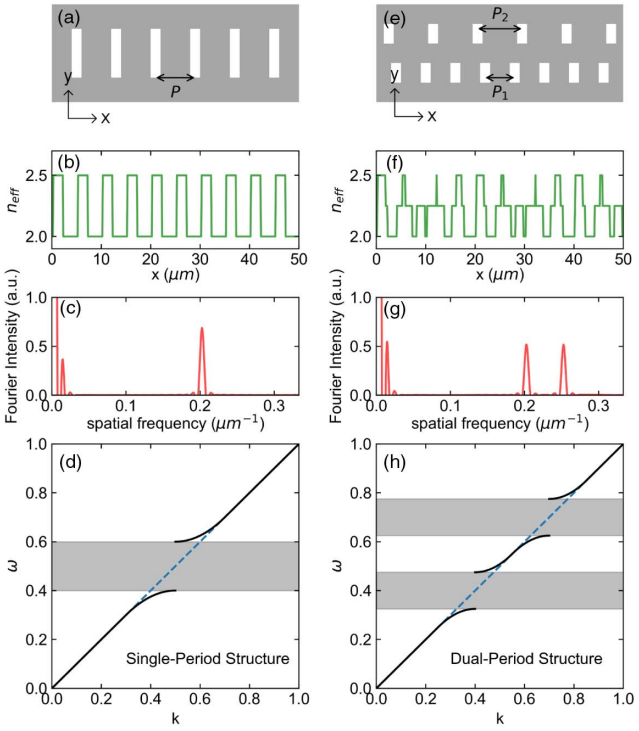

Fig. 1. (a)–(c) Schematic, index profile, spatial frequency spectra, and dispersion of a typical conventional periodic PhC nanobeam. (d)–(f) Schematic, effective refractive index (n_{eff}) profile, spatial frequency spectra, and dispersion of a deterministic PhC aperiodic nanobeam. Note that the dispersions shown here are not accurate and are only for illustration. P, P_1, and P_2 represent the periods of nanobeams.

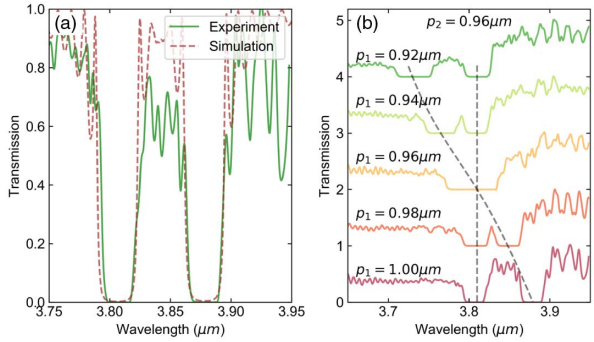

Fig. 2. (a) Numerical and experimental result of transmission of an aperiodic PhC nanobeam. (b) Experimental results with one period varying from 0.92 to 1 μm and the other period fixed at 0.96 μm. The spectra are shifted vertically for clarity, and the black dashed lines are plotted for the guide of the eye to show the shifting of bandgaps.

bandgaps can be designed independently at adjustable wavelengths. The period of one hole array (P_1) varies from 0.92 to 1 μm, while the other (P_2) is fixed at 0.96 μm. In the case that both periods become 0.96 μm, only one bandgap with almost a doubled bandwidth is observed, which is reasonable. Probably due to the limited range of our laser, we do not observe any parasitic bandgaps in experiments. However, simulated results show the existence of parasitic bandgaps in a wider range, similar to previous work [17].

After verifying the multiple bandgaps in the aperiodic PhC nanobeams, we further investigate the possibility of obtaining multiple resonances in a single nanocavity. The nanocavity is created by introducing a phase-delay region in a PhC nanobeam, and the scanning electron microscope (SEM) image is shown at the top of Fig. 3(a). For the experimental results in Fig. 3, the periods of the two arrays of holes are fixed to be 0.92 and 0.98 μm. Figure 3 shows the transmission of a nanocavity with a gap of 2 μm, with two shaded bandgaps. It is obvious that there exists one resonance peak in each bandgap. The Q values are fitted to be 733 and 667 for the resonances at 3.73 and 3.83 μm, respectively. The relatively low Q value is attributed to three reasons: (1) poor confinement due to a small bandgap, (2) material absorption of the SiO_2 substrate, (3) scattering loss because of fabrication imperfection. In order to quantify the respective contributions, the Q values of the two resonances are also simulated, which can be as high as 4554 and 3357, respectively. Therefore, we conclude that fabrication imperfection should be the limiting factor of the Q value.

In Fig. 3(b), we further record the position of resonances for increasing gaps to clarify the reflection response of an aperiodic PhC nanobeam reflector. For resonances in a nanocavity, the wavelength should fulfill the phase-matching condition

$$2\pi\frac{2n_{\text{eff}}\text{Gap}}{\lambda}+2\phi=2N\pi, \tag{3}$$

where λ, n_{eff}, and ϕ are the wavelength in free space, the effective refractive index in the waveguide, and the reflection phase response, respectively. The order of mode is denoted by N. As reported by previous works, for a bandgap in PhC, the reflection phase response changes almost linearly from π to 0 when the wavelength sweeps from the shorter to the longer wavelength edge [18]. Each time that resonance restarts from the shorter wavelength edge, the mode order increases by 1. Based on our results, it appears that this rule also applies to an aperiodic nanobeam with multiple bandgaps. By fitting the experimental data, we can see clearly that the resonances in each bandgap sweep to longer wavelengths for increasing gaps almost linearly, as a result of the linear change of the reflection phase response in the bandgap. Since the reflection response covers a range of π, we can always find a wavelength in the bandgap which meets the resonance equation. Besides, from Eq. (3), the expression of gap difference between adjacent modes can be derived: $\Delta\text{Gap}=\lambda/2n_{\text{eff}}$. The measured gap differences (0.89 and 0.93 μm) also match with the calculated results (0.81 and 0.82 μm). The discrepancy may come from the inaccuracy of linear fitting assumption. Therefore, this Letter suggests that reflection responses in multiple bandgaps of an aperiodic PhC nanobeam also linearly sweep for a range of π independently, when the resonance wavelength shifts from the shorter to the longer wavelength edge. The resonances in an aperiodic PhC nanocavity can still be well described by Eq. (3).

Besides, the mode orders of resonance can also be calculated by Eq. (3). At 3.74 and 3.84 μm, the respective n_{eff} are simulated to be 2.34 and 2.29, and the respective ϕ are estimated to be 0.33π and 0.61π. Then the mode orders of the two resonances at 3.74 and 3.84 μm can be calculated to be 2.8 and 3.0, both of which are closest to the integer of 3. That is, based on Eq. (3), we can ascertain within a certain degree that the mode orders of the two resonances are the same.

Apart from the calculation based on Eq. (3), we also simulated the mode distribution of two resonances to further confirm the matching of mode orders. Figures 4(a)–4(b) show the simulated $Re(E_y)$ at the wavelengths of 3.73 and 3.83 μm, respectively, as shown in Fig. 3(a). The solid white lines represent the borders of the nanobeam, while the white solid rectangles

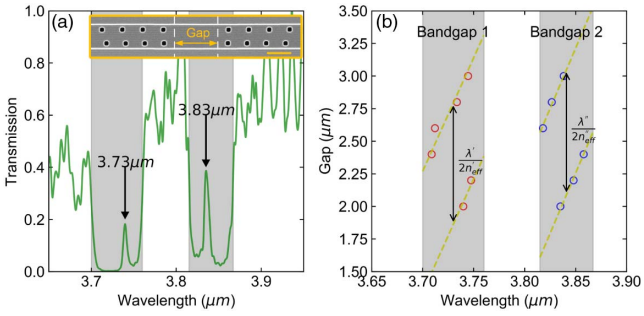

Fig. 3. (a) Measured transmission spectra of an aperiodic PhC nanocavity. P_1 and P_2 are 0.92 and 0.98 μm, respectively. The gap is 2 μm. The inset shows a SEM image of the nanocavity, and the scale bar is 1 μm. (b) Measured positions of resonances for different gaps. The brown lines are the linear fittings of different mode orders. The arrows represent the gap differences between the adjacent modes.

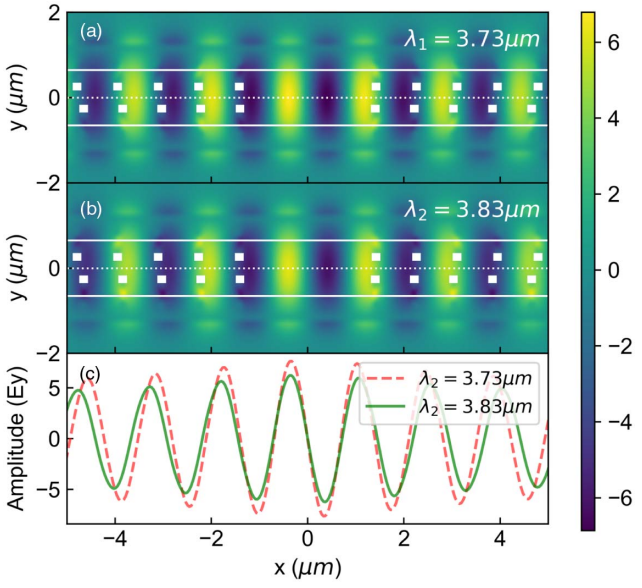

Fig. 4. (a), (b) Electric field (E_y) profiles for the resonances at (a) 3.73 and (b) 3.83 in Fig. 3(a). The solid white lines represent the borders of the nanobeam, while the white solid rectangles denote the etched holes. (c) Electric field (E_y) profiles of two resonances along the dashed lines in (a) and (b).

denote the etched holes. From the figure, both resonances show odd field (E_y) distribution, and the mode orders are both 3, the same as the calculated result. For a better comparison, Fig. 4(c) plots the amplitude of $Re(E_y)$ along the dashed lines in Figs. 4(a) and 4(b). Since the two resonances have the same mode order, they oscillate almost in phase in the gap region, showing nearly perfect field matching. For regions outside the gap, oscillation of the two resonances becomes out of phase gradually, due to the mismatch of the propagating wave vectors. This mismatch could be addressed by using different hole sizes for each resonance. The mismatch is also not critical for applications such as single emitters and nonlinear devices, where the region within the gap is of most importance, since it holds the highest field intensity. To characterize the field match, we define the field-matching factor of two resonances by

$$\eta = \frac{|\int E_1^{\star} E_2 \mathrm{d}A|^2}{\int |E_1|^2 \mathrm{d}A \int |E_2|^2 \mathrm{d}A}, \tag{4}$$

where η, E_1, E_2, are A are the field overlap factor, electric field of the first resonance, electric field of the second resonance, and integral area, respectively. Using Eq. (4), we calculated η of the two resonances in Figs. 4(a) and 4(b) over the gap region to be 99.2%. However, the overlap factor will drop for increasing wavelength mismatch $2(\lambda_1 - \lambda_2)/(\lambda_1 + \lambda_2)$ or gap length, which is a natural result of phase mismatch. According to our calculation, η drops below 90% when the period mismatch exceeds 16% for a fixed gap of 2 μm or when the gap is above 5 μm for two resonances at 3.73 and 3.83 μm.

Before we bring this Letter to its end, it is worth reiterating that we have intentionally designed smaller bandgaps due to the limited range of our laser source. However, a proper bandwidth of the bandgap is important for nanocavities to achieve high Q and good confinement. In order to increase the bandgaps of the aperiodic PhC nanobeams, in addition to the well-known method using an increased hole size, in Fig. 5(a), we show another way by varying the shift factor (SF) of the hole arrays. Here we define the SF to linearly change from 0 and 1 when hole arrays shift from the center line of the nanobeam to the edge. Figures 5(b)–5(f) show the SEM images of samples with different SFs in Fig. 5(a). Since the fundamental transverse electric (TE) mode is involved in our experiment, the field amplitude is strongest at the center of the nanobeam. Therefore, holes closer to the center line of the nanobeam contribute more to the intensity of the Fourier components, and the resultant bandgap is broader. This trend can be obviously seen in Fig. 5(a). When the SF becomes 0, the two bandgaps become so broad that they merge into one.

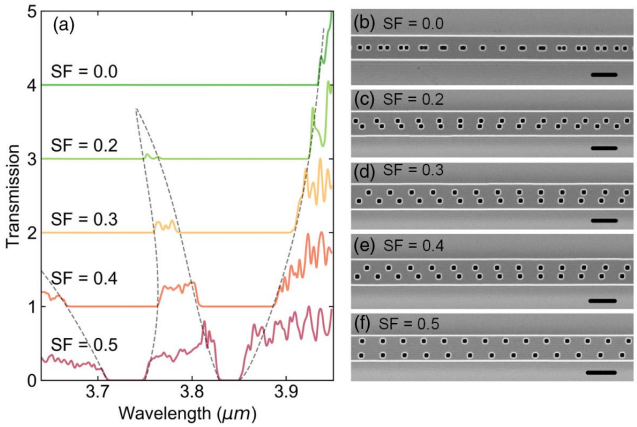

Fig. 5. (a) Measured transmission of aperiodic PhC nanobeams with different SFs (SF). The black dashed lines are drawn to mark the borders of bandgaps for the guide of the eye. (b)–(f) SEM images of the aperiodic PhC nanobeams in (a); the scale bars are 1 μm.

In conclusion, we reported on the design and implementation of deterministic aperiodic PhC nanobeams featuring multiple adjustable bandgaps. The unique property enables the existence of multiple resonances with the same mode order in a single PhC nanocavity. The matching of mode orders is confirmed by both cavity resonance equation and field profile simulation. By merit of the mode matching, the field overlap is almost perfect in the cavity region. We also draw a phenomenological conclusion that in aperiodic PhC nanobeams there is a linear relation between the reflection phase response and the wavelength in each bandgap. The relatively low Q in our proof-of-concept experiments is mainly limited by fabrication imperfection. This Letter offers the opportunities for ultra-compact high-Q nanocavities supporting multiple mode-matched resonances, paving the way to integrated low threshold lasing, compact multiple narrowband emission, and on-chip sensing.

Funding. National Research Foundation Singapore (NRF) (R-263-000-C24-281); China Scholarship Council (CSC) (201706470024).

REFERENCES

1. J. S. Foresi, P. R. Villeneuve, J. Ferrera, E. R. Thoen, G. Steinmeyer, S. Fan, J. D. Joannopoulos, L. C. Kimerling, H. I. Smith, and E. P. Ippen, Nature **390**, 143 (1997).
2. J. J. D. Joannopoulos, S. Johnson, J. N. J. Winn, and R. R. D. Meade, *Photonic Crystals: Molding the Flow of Light* (2008).
3. P. B. Deotare, M. W. McCutcheon, I. W. Frank, M. Khan, and M. Lončar, Appl. Phys. Lett. **94**, 121106 (2009).
4. F. Pyatkov, V. Fütterling, S. Khasminskaya, B. S. Flavel, F. Hennrich, M. M. Kappes, R. Krupke, and W. H. P. Pernice, Nat. Photonics **10**, 420 (2016).
5. K. Y. Jeong, Y. S. No, Y. Hwang, K. S. Kim, M. K. Seo, H. G. Park, and Y. H. Lee, Nat. Commun. **4**, 2822 (2013).
6. J. T. Hill, A. H. Safavi-Naeini, J. Chan, O. Painter, and H. Wang, Nat. Commun. **3**, 1196 (2012).
7. F. Liang and Q. Quan, ACS Photon. **2**, 1692 (2015).
8. P. B. Deotare, L. C. Kogos, I. Bulu, and M. Loncar, IEEE J. Sel. Top. Quantum Electron. **19**, 3600210 (2013).
9. S. Buckley, M. Radulaski, J. L. Zhang, J. Petykiewicz, K. Biermann, and J. Vučković, Opt. Express **22**, 26498 (2014).
10. Q. Quan and M. Loncar, Opt. Express **19**, 18529 (2011).
11. F. Sun, Z. Fu, C. Wang, Z. Ding, C. Wang, and H. Tian, Appl. Opt. **56**, 4363 (2017).
12. M. W. McCutcheon, P. B. Deotare, Y. Zhang, and M. Lončar, Appl. Phys. Lett. **98**, 111117 (2011).
13. P. B. Deotare, M. W. McCutcheon, I. W. Frank, M. Khan, and M. Lončar, Appl. Phys. Lett. **95**, 031102 (2009).
14. Z. V. Vardeny, A. Nahata, and A. Agrawal, Nat. Photonics **7**, 177 (2013).
15. I. Dolev, M. Volodarsky, G. Porat, and A. Arie, Opt. Lett. **36**, 1584 (2011).
16. G. Alagappan and C. E. Png, Nanoscale **7**, 1333 (2015).
17. A. M. Vyunishev, P. S. Pankin, S. E. Svyakhovskiy, I. V. Timofeev, and S. Y. Vetrov, Opt. Lett. **42**, 3602 (2017).
18. E. Istrate and E. H. Sargent, Appl. Phys. Lett. **86**, 151112 (2005).
19. N. Chen, B. Dong, X. Luo, H. Wang, N. Singh, G.-Q. Lo, and C. Lee, Opt. Express **26**, 26242 (2018).